Interplay of epitaxial strain and perpendicular magnetic anisotropy in insulating ferromagnetic $Ga_{1-x}Mn_xP_{1-y}N_y$

P. R. Stone,[1,2,*] L. Dreher,[3] J. W. Beeman,[2] K. M. Yu,[2] M. S. Brandt,[3] and O. D. Dubon[1,2]
[1]*Department of Materials Science & Engineering, University of California, Berkeley, California 94720, USA*
[2]*Lawrence Berkeley National Laboratory, Berkeley, California 94720, USA*
[3]*Walter Schottky Institut, Technische Universität München, Am Coulombwall 3, 85748 Garching, Germany*
(Received 29 January 2010; published 20 May 2010)

We demonstrate a direct connection between the magnetic easy axis in Mn-doped GaP and epitaxial strain by a combined ferromagnetic resonance, x-ray diffraction and superconducting quantum interference device magnetometry study. The magnetic easy axis of $Ga_{1-x}Mn_xP$ is gradually rotated from the in-plane $[0\bar{1}1]$ direction toward the film normal [100] through alloying with isovalent N which changes the strain state of the film from compressive to tensile. For a nearly lattice-matched film the strain-related component to the out-of-plane uniaxial anisotropy field is close to zero. Both in-plane and out-of-plane magnetization reversal processes are explored by a simple model that considers the combination of coherent spin rotation and noncoherent spin switching. We use our results to estimate domain-wall sizes and energetics, which have yet to be directly measured in this materials system. The band structure and electrical properties of $Ga_{1-x}Mn_xP$ imply that holes localized within a Mn-derived impurity band are capable of mediating the same anisotropic exchange interactions as the itinerant carriers in the canonical $Ga_{1-x}Mn_xAs$ system.

DOI: 10.1103/PhysRevB.81.205210 PACS number(s): 75.50.Pp, 76.50.+g, 75.30.Gw, 61.05.cp

I. INTRODUCTION

Intense research efforts in recent years have led to the emergence of Mn-doped III-V semiconductors as promising materials for spintronics.[1] The indirect exchange mechanism between the localized substitutional Mn moments and holes provided by Mn acceptors produces optical, electrical, and magnetic properties that are strongly intertwined, thus providing a framework for the development of novel devices.[2] One specific consequence of the coupling of the electronic and magnetic degrees of freedom is a rich phenomenology of the magnetic anisotropy in $III_{1-x}Mn_xV$ ferromagnetic semiconductors, which is dominated by the epitaxial strain state of the film. In both $In_{1-x}Mn_xAs$ (Refs. 3 and 4) and $Ga_{1-x}Mn_xAs$ (Refs. 5 and 6) the magnetic easy axis tends to lie in the (perpendicular to) the thin-film plane for compressive (tensile) epitaxial strain, though it should be noted that exceptions to this trend have been observed in $Ga_{1-x}Mn_xAs$ with very low hole concentration.[7]

The most widely utilized models of ferromagnetism in $III_{1-x}Mn_xV$ materials are derived from itinerant holes which are described by parameters associated with the host semiconductor's valence band.[8–11] It has been shown that the valence-band model qualitatively and quantitatively reproduces the experimentally observed in-plane to out-of-plane rotation of the easy axis upon changing the strain state from compressive to tensile in $Ga_{1-x}Mn_xAs$.[10–12] Other trends in the magnetic anisotropy of $Ga_{1-x}Mn_xAs$, for example, the carrier concentration dependence of the in-plane uniaxial anisotropy, have also been accounted for by valence-band models.[13] The agreement between the theoretically predicted and empirically determined magnetic easy axes in $Ga_{1-x}Mn_xAs$ is one of the significant achievements of the mean-field description of exchange interactions in ferromagnetic semiconductors. This has taken on greater significance over the past few years as an increasing body of both experimental and theoretical literature has developed suggesting that the holes in $Ga_{1-x}Mn_xAs$ reside not in the valence band but in a separate, Mn-derived impurity band.[14–19]

It is, therefore, of great fundamental interest to examine the magnetic anisotropy in a Mn-doped III-V ferromagnetic semiconductor in which the holes are known to reside in a detached impurity band. One good model system is $Ga_{1-x}Mn_xP$, which displays impurity band physics and robust, carrier-mediated ferromagnetism with reasonably high T_C of up to 65 K for $x=0.042$.[20,21] In this work we show that the epitaxial strain state of $Ga_{1-x}Mn_xP$ plays a significant role in determining the magnetic anisotropy. The strain state of the film is controlled through isovalent alloying of the anion sublattice with N. A similar principle has been previously applied in $Ga_{1-x}Mn_xAs_{1-y}P_y$ grown on GaAs to induce a rotation of the easy axis from in plane to out of plane.[22–24] We find a gradual rotation of the magnetic easy axis from in plane for $Ga_{1-x}Mn_xP$ grown on GaP toward the film normal as the nitrogen fraction of the anion sublattice is increased. The combination of ferromagnetic resonance (FMR) spectroscopy and reciprocal-lattice mapping allows us to directly link the film's strain state to the out-of-plane uniaxial anisotropy field; tensile strain results in an out-of-plane easy axis. Our findings reveal that strain engineering of the magnetic easy axis is possible even when holes are localized within an impurity band.

II. SAMPLE PREPARATION AND STRUCTURAL PROPERTIES

All samples were synthesized using the combination of ion implantation and pulsed-laser melting (II-PLM).[25,26] $Ga_{1-x}Mn_xP$ was synthesized by implantation of 50 keV Mn^+ into (100)-oriented GaP, that is, [100] is the crystallographic direction normal to the film plane, to a dose of 1.5

TABLE I. Relationship between the anion sublattice composition (y), lattice constant (a), vertical strain ($\varepsilon_\perp$), and Curie temperature (T_C) for $Ga_{0.966}Mn_{0.034}P_{1-y}N_y$.

Implanted N^+ dose (cm^{-2})	Approximate y	a (Å)	$\varepsilon_\perp$ (%)	T_C (K)
0.0×10^{15}	0	5.4519 ± 0.0012	0.0220 ± 0.0189	43
1.0×10^{15}	0.004	5.4480 ± 0.0012	-0.0404 ± 0.0202	35
2.5×10^{15}	0.010	5.4456 ± 0.0020	-0.0808 ± 0.0331	35
5.0×10^{15}	0.014	5.4396 ± 0.0024	-0.182 ± 0.0442	35

$\times10^{16}$ cm^{-2} followed by irradiation with a single pulse from a KrF ($\lambda=248$ nm) excimer laser at a fluence of 0.44 ± 0.05 J/cm^2. This produces a $Ga_{1-x}Mn_xP$ film approximately 100 nm thick. Quaternary alloys were synthesized by coimplanting the Mn-implanted GaP with 33 keV N^+ to doses ranging from 1.0×10^{15} to 5.0×10^{15} cm^{-2} prior to PLM. Prolonged (24 h) etching in concentrated HCl was used to remove a very thin highly defective surface layer as well as any surface oxide phases.[25,27]

We define x as the peak Mn_{Ga} concentration[28] and determined it for the $Ga_{1-x}Mn_xP$ reference sample through the dependence of T_C on x, which we have carefully established in previous works.[18,20] The reference sample's T_C of 43 K indicates that $x\approx0.034$. The fraction of Mn atoms substituting Ga (f_{sub}) and retained dose (i.e., the integrated concentration profile) were determined by the combination of channeling Rutherford backscattering spectrometry and particle-induced x-ray emission using $^4He^+$ ions. For all samples we find constant values for f_{sub} and the retained dose of ~77% and $\sim7.29\times10^{15}$ Mn^+/cm^2, respectively which leads us to assign the same value of x to all samples. We observe a negligible concentration of Mn occupying interstitial positions (Mn_I) in all samples; the remainder of the Mn atoms is incommensurate with the lattice. All samples in this work are electrical insulators. A representative resistivity profile for the reference (nitrogen-free) sample can be found in Fig. 2 of Ref. 20. All samples with N show qualitatively similar resistivity profiles, though the magnitude of the resistivity is slightly higher in $Ga_{1-x}Mn_xP_{1-y}N_y$. The T_C for each sample is listed in Table I. Since the Mn composition of all films is the same we attribute the drop in T_C in N containing films to the effect of alloy disorder, which is known to disrupt ferromagnetism in $III_{1-x}Mn_xV$ systems.[18] The N content of the film with the highest N^+ implant dose was determined by measuring the lattice constant of an identically prepared $GaP_{1-y}N_y$ film by x-ray diffraction (not shown). Application of Vegard's law indicates that $y\approx0.014$ for an N^+ implantation dose of 5×10^{15} cm^{-2}. The values of y for other films were estimated from our previous work in the $Ga_{1-x}Mn_xAs_{1-y}N_y$ system[18] and are shown in Table I. We note that exact determination of y is not essential to the strain analysis of the magnetic anisotropy. The epitaxial strain is explicitly calculated below.

Reciprocal-lattice maps for the samples with $y=0$, $y=0.004$, and $y=0.014$ taken around the (511) diffraction peak are shown in Fig. 1. Measurements were performed using

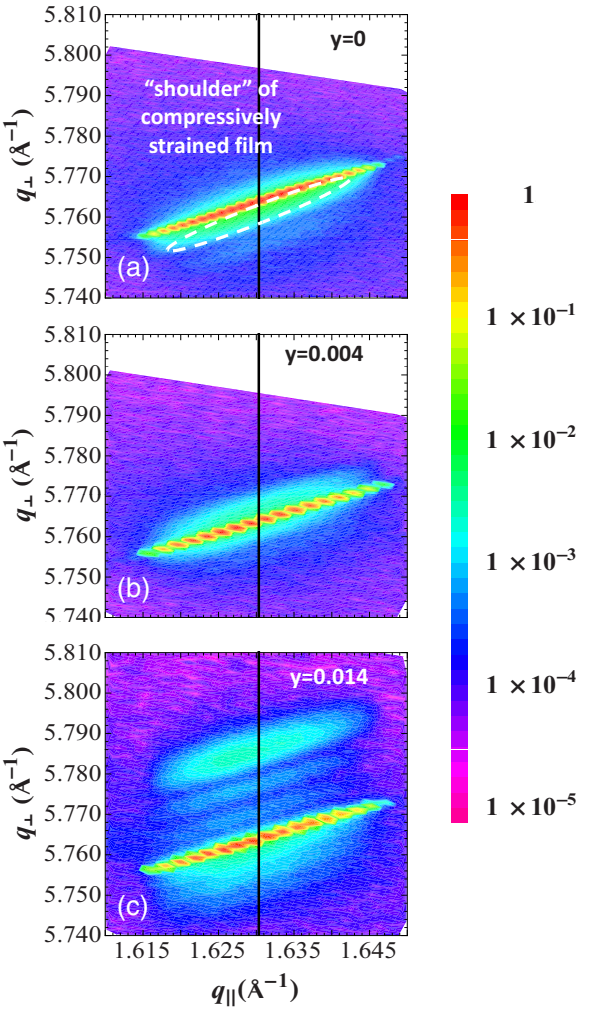

FIG. 1. (Color online) Reciprocal-lattice maps around the (511) diffraction peak for $Ga_{0.966}Mn_{0.034}P_{1-y}N_y$ samples with (a) $y=0$ (b) $y=0.004$, and (c) $y=0.014$. The solid line at $q_{||}=1.6303$ Å^{-1} corresponds to the equilibrium lattice constant of GaP, which is present to emphasize that the films are pseudomorphic with the underlying substrate.

Cu $K\alpha$ radiation ($\lambda=1.5405$ Å) with line focusing. The sample with $y=0$ shows significant intensity in a diffuse region at slightly smaller perpendicular reciprocal-lattice vector ($q_\perp$) than the main GaP substrate peak. We attribute this feature to the pseudomorphic $Ga_{1-x}Mn_xP$ thin film in analogy to annealed $Ga_{1-x}Mn_xAs$ films grown by low-temperature molecular beam epitaxy (LT-MBE) on GaAs in which the films are observed to be in compressive strain.[12,23] We observe a shoulder instead of a peak due to the nonuniform Mn distribution throughout the depth of the film which is inherent to II-PLM processing of Mn-doped III-V semiconductors at these large doping levels.[29] The vertical concentration gradient gives rise to a gradient in perpendicular interplanar spacing which prevents the resolution of a distinct film peak. Replacement of ~1.4% of the anion sublattice in $Ga_{0.966}Mn_{0.034}P$ with N causes the strain state of the film to change from compressive to tensile, which is illustrated in Fig. 1(c). The significantly smaller N anions easily reverse the strain to the point where the film peak is easily

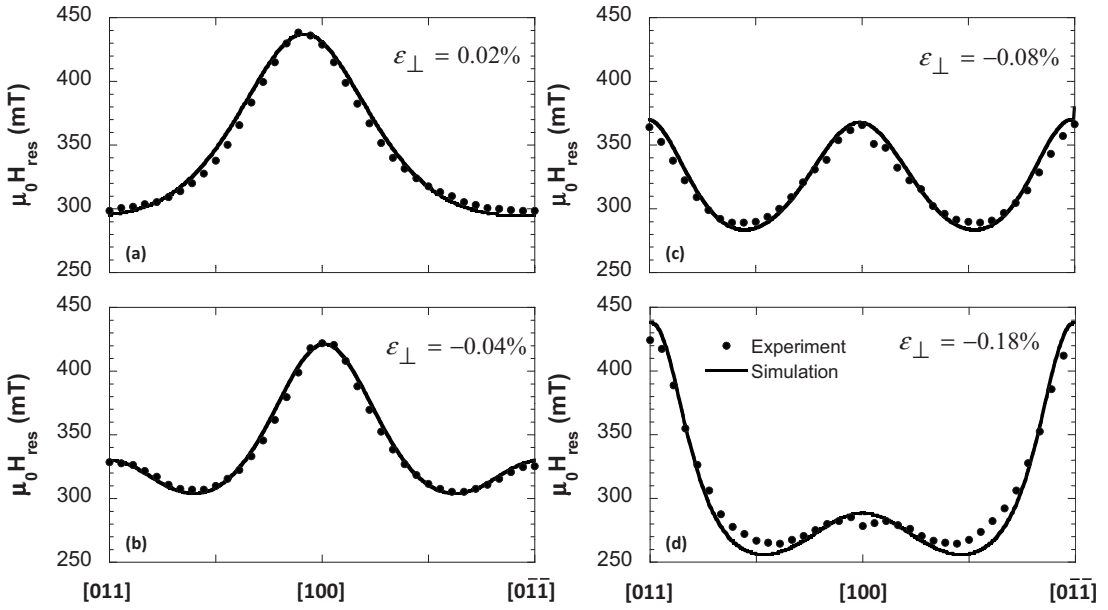

FIG. 2. [(a)–(d)] Dependence of the ferromagnetic resonance field on orientation for rotations in the $(0\bar{1}1)$ plane for $Ga_{0.966}Mn_{0.034}P_{1-y}N_y$. The FMR data were acquired at $T=5$ K using a microwave frequency $\omega/2\pi \approx 9.26$ GHz. Symbols represent experimental data while the solid lines are fits according to the model described in the text.

resolved although the vertical inhomogeneity gives rise to significant broadening. A small, residual feature at $q_\perp$ below the substrate peak arises from the imperfect overlap of the Mn and N profiles which leaves a small portion of the film compressively strained even though the majority of the film is under tensile strain.

While the broadening of the film diffraction peaks hinders quantitative analysis of the reciprocal-lattice maps, it is still possible to extract in-plane ($a_\parallel$) and out-of-plane ($a_\perp$) lattice constants. For the $y=0.014$ and $y=0.010$ films (reciprocal-lattice map not shown), the analysis is straightforward as the film diffraction peak is distinguishable from the substrate. We use the values of $q_\parallel$ and $q_\perp$ at the film peak to determine $a_\parallel$ and $a_\perp$. Errors in $a_\perp$ are determined by the full width at half maximum contour. For the films with $y=0.004$ and $y=0$ it is assumed that $a_\parallel = a_{GaP} = 5.4505$ Å, which is reasonable given the small lattice mismatch in these films. We note that the film with $y=0.014$ is still pseudomorphic despite the larger mismatch compared to the films with $y=0$ and $y=0.004$, which provides justification for this assumption. The individual ω-2θ scans comprising the reciprocal-lattice maps for samples with $y=0$ and $y=0.004$ were fit using a two-peak model wherein the substrate peak is modeled by a combined Gaussian-Lorentzian function[30] and the film by a Gaussian distribution. Modeling of ω-2θ scans for the sample with $y=0.014$ showed that the resolved film peak is well described by a Gaussian, which justifies our use of a Gaussian function to describe the dependence of the diffracted intensity on reciprocal-lattice vector. The mean film perpendicular lattice constant was determined from the mean of the film's Gaussian function and errors quoted as the full width at half maximum of the distribution.

In all cases the relaxed lattice constant, a, was calculated by

$$a = \frac{a_\perp + 2a_\parallel \nu - a_\perp \nu}{1+\nu}, \tag{1}$$

where ν is Poisson's ratio and is 0.31 for GaP, which is assumed to be unchanged by dilute alloying with Mn or N.[31] The relaxed lattice constant as well as the strain along the growth direction, $\varepsilon_\perp = (a_\perp - a)/a$, are listed as a function of N concentration in Table I. Samples will be referred to by their strain for the remainder of this paper. These calculations reflect the trends discussed qualitatively above, particularly the change in the strain state with N alloying.

III. MEASUREMENTS OF THE MAGNETIC ANISOTROPY

A. Ferromagnetic resonance spectroscopy

Figure 2 shows the dependence of the ferromagnetic resonance field ($\mu_0 H_{res}$) on the orientation of the applied magnetic field for rotations about the $[0\bar{1}1]$ axis. The FMR measurements were performed at $T=5$ K using a microwave frequency $\omega/2\pi \approx 9.26$ GHz. In-plane rotations for all films (not shown) were all qualitatively similar with local minima for $H \parallel \langle 011 \rangle$ and local maxima for $H \parallel \langle 001 \rangle$ which confirmed that the $\langle 011 \rangle$-type directions were the easy axes in the plane of the film. A small uniaxial term breaks the symmetry between [011] and $[0\bar{1}1]$ directions; the $[0\bar{1}1]$ direction is magnetically preferred to [011].[29,32] The magnitude of this uniaxial anisotropy field is ≤ 5 mT for all samples, which is significantly less than the other anisotropy fields. Therefore, even though the FMR rotations shown in Fig. 2 have $H \parallel [011]$ for the in-plane orientation of the magnetic field we can still assess reasonably from these rotations whether the magnetic easy axis lies in plane or perpendicular to the plane. For the sample under compressive strain the resonance

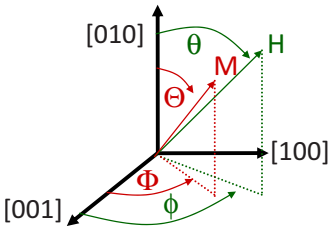

FIG. 3. (Color online) Coordinate system used for FMR and $M(H)$ simulations. Capital letters refer to the magnetization vector while lowercase letters refer to the orientation of the applied magnetic field. The [100] direction is perpendicular to the plane of the thin film.

field is at a minimum for in-plane orientations and a maximum for the out-of-plane [100] demonstrating that the magnetic easy axis is in the plane of the film. For the film under the most tensile strain [panel (d) of Fig. 2] the maximum resonance field now occurs for $H\|[011]$, which indicates that the film plane is magnetically hard. The minimum in the angular dependence of $\mu_0 H_{\text{res}}$ gradually shifts from in plane toward the film normal as the lattice constant decreases though the magnetic easy axis is still not parallel to [100] at $\varepsilon_\perp = -0.18\%$.

For a more quantitative interpretation of the FMR data, simulations of the angular dependence of the FMR were performed. We write the free energy F as a function of the orientations of the applied magnetic field and sample magnetization vector taking into account energies due to the Zeeman effect and anisotropy,

$$\begin{aligned} F = &- MH(\sin\Theta\sin\Phi\sin\theta\sin\phi + \cos\Theta\cos\theta \\ &+ \sin\Theta\cos\Phi\sin\theta\cos\phi) + K_{eff}^{100}\sin^2\Theta\sin^2\Phi \\ &- \frac{1}{2}K_{c1}^{\perp}\sin^4\Theta\sin^4\Phi - \frac{1}{2}K_{c1}^{\|}(\cos^4\Theta + \sin^4\Theta\cos^4\Phi) \\ &+ \frac{1}{2}K_u^{011}(\cos\Theta + \sin\Theta\cos\Phi)^2. \end{aligned} \tag{2}$$

In Eq. (2) θ, ϕ and Θ, Φ define the orientation of the magnetic field and magnetization vectors, respectively, according to the coordinate system shown in Fig. 3. The parameter K_{eff}^{100} describes uniaxial magnetic anisotropy normal to the film and is the sum of shape and epitaxial strain-related terms, which have the same angular dependence and therefore cannot be separated. $K_{c1}^{\|}$ and $K_{c1}^{\perp}$ are cubic terms representative of a tetragonally distorted film. Finally, K_u^{011} accounts for the inequivalence of in-plane $\langle 011\rangle$-type directions.[29,32]

Following the approach of Smit *et al.*,[33,34] we obtain the equation of motion

$$\left(\frac{\omega}{\gamma}\right)^2 = \frac{1}{M^2\sin^2\Theta}\left[\left(\frac{\partial^2}{d\Phi^2}F\right)\left(\frac{\partial^2}{\partial\Theta^2}F\right) - \left(\frac{\partial}{\partial\Phi}\frac{\partial}{\partial\Theta}F\right)^2\right]_{\Phi_0,\Theta_0}, \tag{3}$$

where $\gamma = g\mu_B/\hbar$ is the gyromagnetic ratio. Equation (3) is evaluated at the equilibrium orientation of the magnetization, which is found by the minimization conditions,

TABLE II. Cubic and uniaxial magnetic anisotropy fields determined from FMR.

$\varepsilon_\perp$ (%)	$2K_{eff}^{100}/M$ (mT)	$2K_{c1}^{\perp}/M$ (mT)	$2K_{c1}^{\|}/M$ (mT)	$2K_u^{011}/M$ (mT)
0.0220 ± 0.0189	78 ± 3	-26 ± 3	-24 ± 3	5 ± 1
-0.0404 ± 0.0202	4 ± 3	-84 ± 3	-34 ± 3	4 ± 1
-0.0808 ± 0.0331	-80 ± 3	-116 ± 3	-38 ± 3	3 ± 1
-0.182 ± 0.0442	-172 ± 3	-124 ± 3	-40 ± 3	4 ± 1

$$\left.\frac{\partial}{\partial\Phi}F\right|_{\Phi=\Phi_0} = \left.\frac{\partial}{\partial\Theta}F\right|_{\Theta=\Theta_0} = 0. \tag{4}$$

The simultaneous solution of Eqs. (3) and (4) yields the FMR resonance condition at a specific magnetic field orientation.

Results of the FMR simulations are shown by the solid lines in Fig. 2 using parameters that fall within the range of anisotropy fields listed in Table II. The simulations also fit in-plane rotations of the samples. The in-plane anisotropy fields are only weakly dependent on the strain state of the film. We note that the small uniaxial anisotropy field $2K_u^{011}/M$ is positive for all $\varepsilon_\perp$. This, along with the constantly negative sign of $2K_{C1}^{\|}/M$, signifies that $[0\bar{1}1]$ is the in-plane easy axis for all samples. The out-of-plane anisotropy fields show a much stronger dependence on the film strain and dominate the behavior of the magnetic anisotropy in all films. In particular, the effective uniaxial out-of-plane anisotropy $2K_{eff}^{100}/M$ is correlated with both the sign and magnitude of $\varepsilon_\perp$. The linear dependence of $2K_{eff}^{100}/M$ on $\varepsilon_\perp$ is emphasized in Fig. 4. Linear behavior is also observed in $Ga_{1-x}Mn_xAs$ for both compressive and tensile strains up to 0.4% (Ref. 12) suggesting a common origin to this effect in the two materials systems. From the linear regression, we

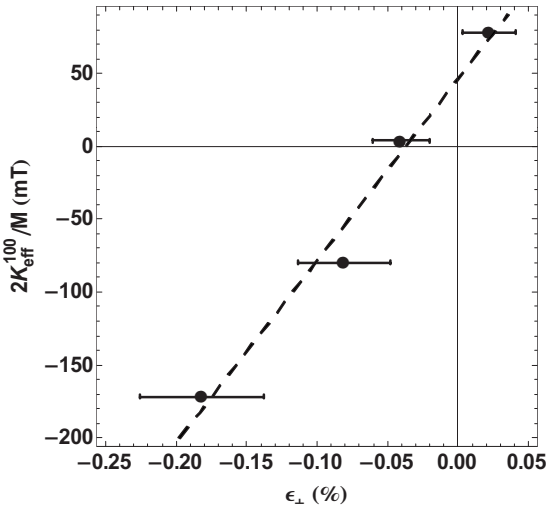

FIG. 4. Dependence of the FMR-derived out-of-plane effective uniaxial anisotropy field $2K_{eff}^{100}/M$ on $\varepsilon_\perp$. The dashed line is a linear fit to the data points, which intercepts the ordinate axis at $2K_{eff}^{100}/M \approx 46$ mT.

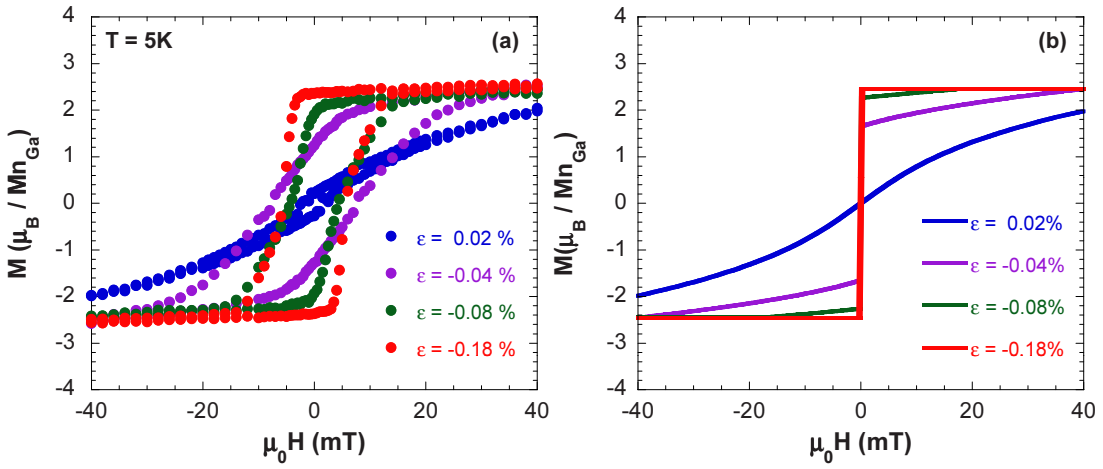

FIG. 5. (Color online) (a) Field dependence of the magnetization of $Ga_{0.966}Mn_{0.034}P_{1-y}N_y$ for $H\|[100]$. (b) $M(H)$ simulations for $H\|[100]$ according to the model described in the text. Specific values for the set of anisotropy fields ($2K_{eff}^{100}/M$, $2K_{c1}^{\perp}/M$, $2K_{c1}^{\|}/M$, and $2K_u^{011}/M$) used in the simulations were (60, −64, −52, and 5 mT) for $\varepsilon_\perp=0.02\%$, (−18, −60, −40, and 4 mT) for $\varepsilon_\perp=-0.04\%$, (−84, −98, −40, and 3 mT) for $\varepsilon_\perp=-0.08\%$, and (−222, −164, −40, and 4 mT) for $\varepsilon_\perp=-0.18\%$.

estimate that $2K_{eff}^{100}/M \approx 46$ mT for $\varepsilon_\perp=0$. High-field ($1 \leq |\mu_0 H| \leq 5$ T) superconducting quantum interference device (SQUID) magnetometry measurements indicate that the saturation magnetization $M_{sat}=26.1\pm2.1$ kA/m (to obtain the magnetization in units of A/m we have used the method outlined in Appendix B of Ref. 32), which implies a demagnetization field $\mu_0 M_{sat}$ of 32.8 ± 2.6 mT, which accounts for a significant portion of $2K_{eff}^{100}/M$ at $\varepsilon_\perp=0$. Therefore, within the error bar of our strain measurements, we conclude that for a nearly lattice-matched film the component of $2K_{eff}^{100}/M$ due to epitaxial strain is close to zero for $Ga_{1-x}Mn_xP$.

B. Field dependence of the magnetization

Figure 5(a) shows the field dependence of the magnetization, $M(H)$, at $T=5$ K for all samples when the external magnetic field was applied perpendicular to the film. For the sample in compressive strain no remanence is observed since the magnetic easy axis is perpendicular to [100] (in the film plane). As the strain of the film devolves from compressive to tensile the remanent magnetization of the film increases gradually as the magnetic easy axis rotates from $[0\bar{1}1]$ to [100]. In parallel the line shape of the $M(H)$ curves evolves. As the film is put into increasing tensile strain hysteresis develops, and the curves develop the more squarelike loops characteristic of magnetization reversal for easy directions.

To gain further insight into the magnetization reversal processes in $Ga_{1-x}Mn_xP_{1-y}N_y$ the in-plane and out-of-plane $M(H)$ curves for all samples have been simulated using a free-energy approach. Details of these calculations can be found elsewhere.[29] Simulations of the out-of-plane magnetization curves for all samples are shown in Fig. 5(b). For simplicity and clarity we have neglected the effects of hysteresis in these simulations but will return to those effects later. The central features of the experimental $M(H)$ curves are reproduced well by this simple model, namely, the increase in the remanent magnetization with increasing tensile strain and the general change in line shape of the $M(H)$ curve. The specific values for the anisotropy parameters used in each simulation are given in the caption of Fig. 5. In general, the anisotropy fields used for simulation of the $M(H)$ curves agree with those determined from FMR simulations to better than a factor of 2. This level of agreement is quite reasonable given that we observed spin-wave excitations in both the in-plane and out-of-plane FMR spectra. The anisotropy parameters listed in Table II were determined by analyzing the angular dependence of the fundamental mode. A complete analysis of the spin-wave excitations is both beyond the scope of this work and also quite challenging since only one or two higher order modes were observed. We note only that the presence of spin waves can cause an underestimation of the resonance field corresponding to the collective mode, which may explain some of the discrepancy between the anisotropy parameters determined from the FMR and SQUID simulations.[35] Regardless, the anisotropy fields determined from $M(H)$ calculations further emphasize that the sign and magnitude of $2K_{eff}^{100}/M$ are determined primarily by the epitaxial strain of the film.

We now turn our attention to the out-of-plane magnetization reversal process for $Ga_{1-x}Mn_xP_{1-y}N_y/GaP$ films. The simulations indicate that the magnetization vector is always of the form $[uv\bar{v}]$ during the reversal process, which can be understood as follows. As the magnitude of the magnetic field is reduced the Zeeman energy decreases. Since none of the samples have an easy axis parallel to [100], eventually the anisotropy energy will cause the magnetization to bend toward the sample plane. The lowest-energy path is that toward the in-plane easy axis, which is $[0\bar{1}1]$. Therefore, reversal occurs in the (011) plane, which is common to both [100] and $[0\bar{1}1]$ directions. To aid in the visualization of the magnetization reversal process in the (011) plane we change coordinates such that the magnetization can be described by a single angle. We define γ as the angle in the (011) plane as measured from [100] toward $[01\bar{1}]$ [Fig. 6(a)]. Describing the magnetization by this single angle we can rewrite Eq. (2) as

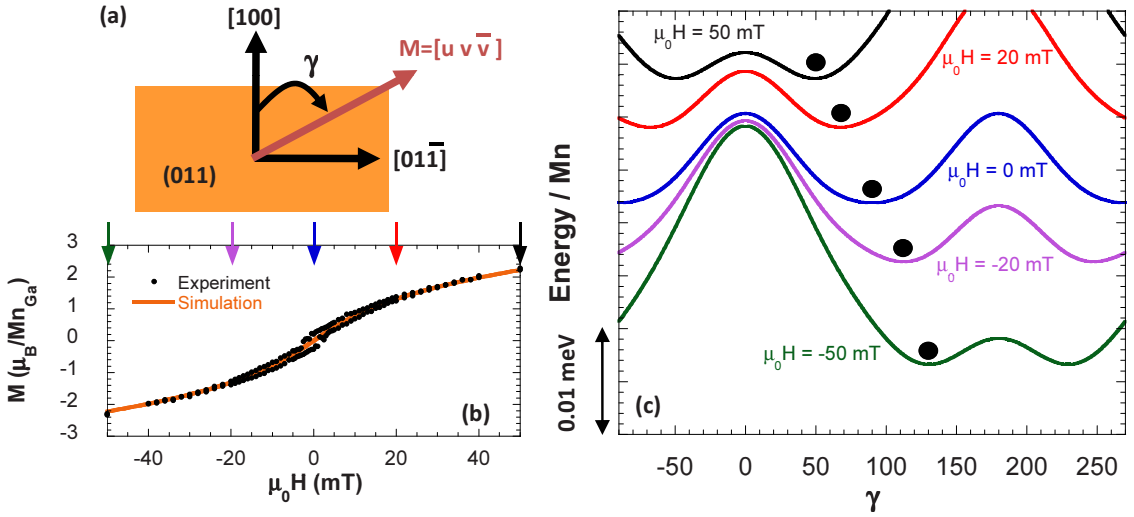

FIG. 6. (Color online) (a) Definition of the angle γ in the (011) plane. (b) Comparison of experimental (symbols) and calculated (solid line) $M(H)$ curves for the sample with $\varepsilon_\perp = 0.02\%$. Anisotropy parameters are the same as those used in Fig. 5. The arrows refer to the individual $F(\gamma)$ curves in panel (c). (c) Free energy as a function of the angle of the magnetization vector in the (011) plane. The solid, filled circles denote the minimum in the free-energy curve, and therefore the orientation of the magnetization at the specified field. The two minima visible in some of the curves are equivalent by symmetry and do not affect the results of the simulations.

$$F(\gamma) = -MH\cos(\gamma) + K_{eff}^{100}\cos^2(\gamma) - \frac{K_{c1}^{\perp}}{2}\cos^4(\gamma) - \frac{K_{c1}^{\parallel}}{4}\sin^4(\gamma), \quad (5)$$

when $H \| [100]$. Out-of-plane $M(H)$ simulations for the compressively strained $Ga_{0.966}Mn_{0.034}P/GaP$ structure ($\varepsilon_\perp = 0.02\%$) are shown in Fig. 6 alongside the $F(\gamma)$ contours for specified values of the magnetic field. As the field is swept from positive to negative values, the minimum in the $F(\gamma)$ curves shifts gradually from $\gamma = 0°$ to $\gamma = 180°$ indicating that magnetization process is completely reversible and occurs by coherent rotation of the magnetization vector.

The mechanism for magnetization reversal is markedly different for films under tensile strain. Experimental and calculated $M(H)$ curves for the film with $\varepsilon_\perp = -0.18\%$ are shown in Fig. 7. In this case as the field is lowered from a large positive value toward zero, the magnetization stays pinned near $\gamma = 0°$ since the magnetic anisotropy energy induces the magnetization to lie close to [100] at zero field. Since the minimum does not gradually shift past $\gamma = 90°$, the only mechanism whereby the magnetization can change sign is noncoherent switching. The noncoherent switch occurs when the energy gained by switching from the local minimum in $F(\gamma)$ to the global minimum is sufficient to account for the energy necessary for domain nucleation and growth, ΔE. For the simulation shown in Fig. 7, it was assumed that $\Delta E = 2.01 \times 10^{-3}$ meV/Mn which causes the noncoherent spin flips to occur at ± 7 mT in reasonable agreement with the experiment. As we have noted in a previous paper,[29] the simulations produce noncoherent spin switches which are much sharper than those that are observed in experiment. The reasons for this are twofold. On the one hand the simple model neglects some processes, such as the pinning and de-

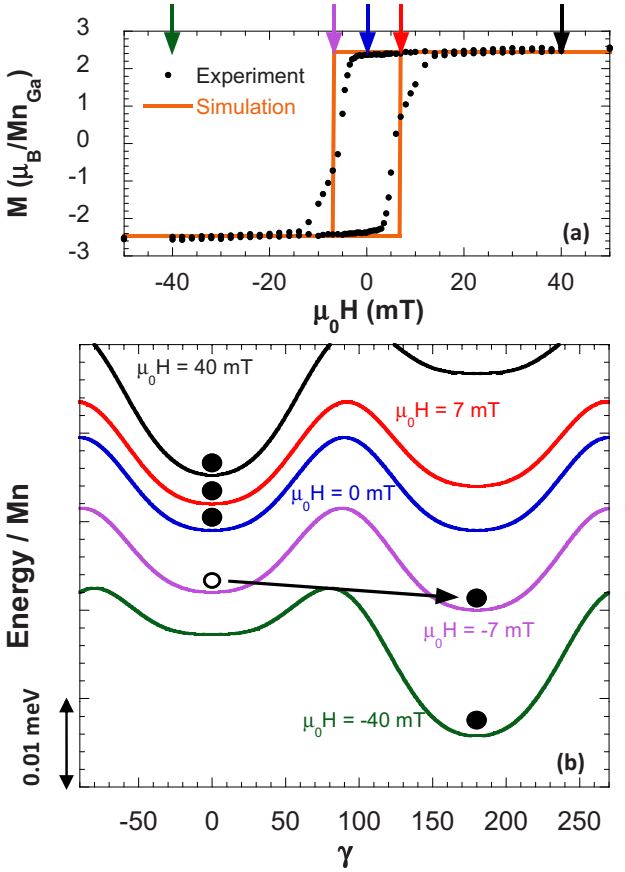

FIG. 7. (Color online) (a) Comparison of simulated and experimental out-of-plane hysteresis loops for the $Ga_{0.966}Mn_{0.034}P_{1-y}N_y$ film with $\varepsilon_\perp = -0.18\%$ and for a single value of ΔE. (b) Free energy as a function of the orientation of the magnetic moment in the (011) plane at selected magnetic field strengths.

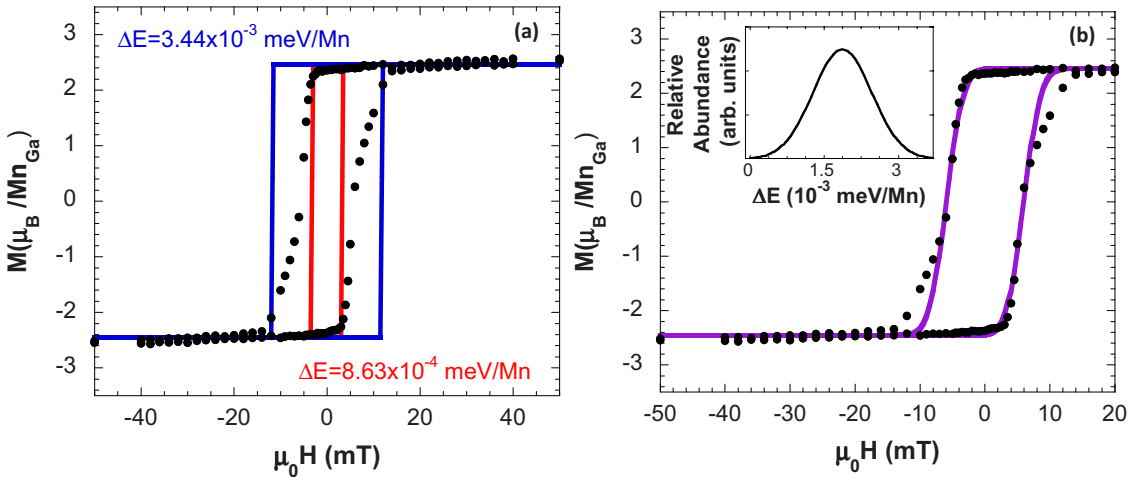

FIG. 8. (Color online) (a) Simulations of the $M(H)$ curves (solid lines) for the sample with $\varepsilon_\perp = -0.18\%$ using a single value for ΔE. Experimental data points are shown by the black solid symbols. The two simulated curves place upper and lower bounds for the value of ΔE according to the single-valued model. (b) Comparison of experimental (symbols) and simulated (solid line) $M(H)$ curves for the same sample using a Gaussian distribution of ΔE. The Gaussian distribution is centered at $\Delta E = 1.9 \times 10^{-3}$ meV/Mn with $\sigma = 0.60 \times 10^{-3}$ meV/Mn and is shown in the inset.

pinning of domain walls by materials defects, which can affect the shape of the $M(H)$ loops. Second, the model assumes that the material is completely homogeneous and well described by single-valued parameters for both the magnetic anisotropy (set of K) and the hysteretic processes (ΔE). Nonuniform distribution of the Mn moments and materials defects can result in local fluctuations in the magnetization and carrier concentration which can affect both the magnetic anisotropy and reversal process, thus giving rise to the differences in experimental and calculated hysteresis loops. We can put error bars on the value of ΔE extracted from our single-valued model by "bounding" the experimental $M(H)$ curves with simulated ones as is shown in Fig. 8(a). From these simulations we identify the approximate range $0.863 \times 10^{-3} \leq \Delta E \leq 3.44 \times 10^{-3}$ meV/Mn for the energy required for domain nucleation and growth for the sample with $\varepsilon_\perp = -0.18\%$. We can also improve our model by taking into account local fluctuations in the magnetic anisotropy and assuming that ΔE is not single valued but instead takes on a distribution of values throughout the sample. In accordance with the procedure of Refs. 29 and 36 the distribution in ΔE is assumed to be Gaussian. Figure 8(b) compares the experimental $M(H)$ curve with a simulation assuming a Gaussian distribution of ΔE centered around 1.9×10^{-3} meV/Mn with a standard deviation of 6.0×10^{-4} meV/Mn. The agreement between experiment and simulation is greatly improved assuming the Gaussian distribution of ΔE indicating that local fluctuations in x, p, and/or defect concentrations have a significant effect on the magnetic anisotropy and magnetization reversal. As a point of reference we note that Liu *et al.*[37] found that $\Delta E \approx 5.5 \times 10^{-3}$ meV/Mn in $Ga_{0.98}Mn_{0.02}As$ thin films with out-of-plane easy axis, which is of similar magnitude to the values reported here for $Ga_{1-x}Mn_xP_{1-y}N_y$. However, comparison is limited since the $Ga_{1-x}Mn_xP_{1-y}N_y$ film with $\varepsilon_\perp = -0.18\%$ has nearly a factor of 2 larger x and its easy axis is not completely out of plane.

We estimate the energy of a Bloch domain wall per unit area following the standard treatment[37,38] as

$$\sigma_w = 2\pi\sqrt{\frac{\Delta E S^2 J}{d}}, \tag{6}$$

where J is the exchange energy, $d = ax^{-1/3}$ is the average spacing between Mn atoms, and ΔE is in units of joules per cubic meter. Following Refs. 37 and 39, we assume $J = 3k_B T_C / 2zS(S+1)$, where $S = 5/2$ for Mn^{2+} ions and $T_C = 35$ K for the film with $\varepsilon_\perp = -0.18\%$. As pointed out in Ref. 39, the number of nearest-neighbor spins z is not well defined for a system of random magnetic dopants in a zinc-blende lattice; so we take $4 \leq z \leq 12$ which introduces a source of error. Within these approximations we find that $0.013 < \sigma_w < 0.032$ erg/cm^2 $(1.31 \times 10^{-5} < \sigma_w < 3.17 \times 10^{-5}$ J/m$^2)$ which is close to the value of 0.027 erg/cm^2 reported for $Ga_{0.98}Mn_{0.02}As$ established by a similar method.[37] On the other hand Gourdon *et al.*[40] determined a much larger value of $\sigma_w \approx 0.2$ erg/cm^2 from domain theory for $Ga_{0.93}Mn_{0.07}As$ grown in tensile strain. The range of domain parameters determined for $Ga_{1-x}Mn_xAs$ of different compositions underscores the need to compare materials of nearly identical x, p, and $\varepsilon_\perp$ since the magnetic anisotropy depends strongly on these quantities. Thus, further studies are necessary in order to establish trends in the domain parameters between $Ga_{1-x}Mn_xAs$ and $Ga_{1-x}Mn_xP$.

IV. DISCUSSION

The ability to strain engineer an out-of-plane magnetic easy axis in $Ga_{1-x}Mn_xP$ will allow for the exploration of new experiments that will increase understanding of this system. An out-of-plane easy axis enhances contrast in techniques such as spatially resolved magneto-optic Kerr effect microscopy, which has been used previously to image both the domain structure and domain dynamics during magnetization reversal.[41,42] In addition to visualizing the domain structure these measurements provide complimentary information regarding the magnetic anisotropy. Application of micromag-

netic theory would allow us to assess and refine the predictions regarding magnetic domains in $Ga_{1-x}Mn_xP$ extracted from the simple free-energy model as well as determine other important parameters such as the spin stiffness constant, which has yet to be experimentally determined in $Ga_{1-x}Mn_xP$.[40]

Perhaps more importantly, detailed knowledge of magnetic anisotropy in $Ga_{1-x}Mn_xP$ has important ramifications toward fundamental understanding of the exchange interactions in Mn-doped III-V semiconductors. We have previously examined in depth the magnetic anisotropy of compressively strained $Ga_{1-x}Mn_xP$ films.[32] For $Ga_{1-x}Mn_xP$ as in $In_{1-x}Mn_xAs$,[43] the in-plane easy axis is parallel $\langle 011 \rangle$ at all temperatures (negative $2K_{C1}^{\parallel}/M$). In $Ga_{1-x}Mn_xAs$ both positive and negative $K_{C1}^{\parallel}$ have been observed. In some samples $\langle 001 \rangle$ axes are magnetically preferred by cubic symmetry[5,44] while more recently $\langle 011 \rangle$-type magnetic easy axes have been observed in $Ga_{1-x}Mn_xAs$ samples in which compensation is low.[45,46] The oscillatory nature of $K_{C1}^{\parallel}$ is expected based on the Zener model.[10] While such oscillatory behavior has not been observed in $Ga_{1-x}Mn_xP$, we have explored only a small range of Mn doping, and compensation in our magnetic anisotropy experiments. We have previously shown that $K_{C1}^{\parallel}$ is weakly dependent on compensation in $Ga_{1-x}Mn_xP_{1-y}S_y$.[29] Thus, it is possible that the sign of the cubic anisotropy field may differ for a certain range of x, p in $Ga_{1-x}Mn_xP$ and further studies are needed to explore this possibility.

All three materials systems show an in-plane uniaxial anisotropy term ($2K_u^{011}/M$) that breaks the symmetry between $\langle 011 \rangle$ directions.[3,32,47] The in-plane uniaxial anisotropy is essentially independent of film strain in both $Ga_{1-x}Mn_xP$ (this work) and $Ga_{1-x}Mn_xAs$.[13] The symmetry breaking mechanism that gives rise to this uniaxial term has not been conclusively established. The effect is likely intrinsic to ferromagnetic semiconductors since it is independent of both thickness[13] and processing.[48,49] The notion of layer-by-layer continuance of solid/vacuum surface reconstructions seeded at the original interface during LT-MBE growth[50] should be reconsidered since comparable reconstructions are unlikely to occur during liquid phase regrowth.[48,49]

A recent study confirmed that the magnetic anisotropy of II-PLM formed $Ga_{1-x}Mn_xAs$ is substantially similar to $Ga_{1-x}Mn_xAs$ produced by LT-MBE,[49] which justifies comparison between materials produced by different growth techniques. This is important since almost all studies of the magnetic anisotropy in $III_{1-x}Mn_xV$ materials have been performed on samples synthesized by LT-MBE while the magnetic anisotropy of $Ga_{1-x}Mn_xP$ has been studied on materials formed by II-PLM. Comparing to the results of Glunk *et al.* obtained on LT-MBE formed $Ga_{0.95}Mn_{0.05}As$ we find that $2K_{eff}^{100}/M$ for our $Ga_{1-x}Mn_xP_{1-y}N_y$ films is of similar magnitude for both compressive and tensile strain implying that the perpendicular magnetic anisotropy is not strongly affected by the host semiconductor. On the other hand, Zhou *et al.*[49] obtained $2K_{eff}^{100}/M \approx 166$ mT for $Ga_{0.96}Mn_{0.04}As$ formed by II-PLM. While this value is nearly a factor of two greater than that reported here for a $Ga_{1-x}Mn_xP$ film with similar x we note that the strain of the film was not determined in Ref. 49, which is the primary factor in determining $2K_{eff}^{100}/M$. Ideally in order to quantify the effect of changing the host semiconductor from GaAs to GaP on the magnitude of the perpendicular magnetic anisotropy one should compare samples with nearly identical compositional and strain parameters. Further studies are clearly needed to elucidate what quantitative effect, if any, changing the host semiconductor has on the magnitude of the perpendicular magnetic anisotropy field.

Although the low-temperature easy axes may be different in compressively strained $Ga_{1-x}Mn_xAs$ and $Ga_{1-x}Mn_xP$, one can control the magnetic easy axis in the same manner in the two materials. In $Ga_{1-x}Mn_xAs$ the sign and magnitude of the in-plane uniaxial anisotropy field $2K_u^{011}/M$ is strongly dependent on the carrier concentration while that of $2K_{eff}^{100}/M$ depends on the epitaxial strain. As alluded to in Sec. I mean-field, valence-band theory reproduced this behavior by explicitly considering strain terms in the p-d exchange augmented $\mathbf{k}\cdot\mathbf{p}$ Hamiltonian. In these models the magnetic anisotropy arises due to the $\mathbf{k}$ dependence of the hole dispersion, which through the p-d exchange interaction causes the energy of the entire Mn-hole system to depend on the orientation of the Mn moments relative to the crystallographic axes. The strain dependence of the anisotropy then arises due to further splitting of the spin-split light-hole and heavy-hole valence bands, which causes a redistribution of the spin-polarized holes and therefore can change the orientation of the magnetic easy axis. In this formalism the p dependence of the in-plane uniaxial anisotropy is consistent with a small shear ε_{xy} term while the out-of-plane anisotropy can be explained by biaxial strain terms. The evolution of the magnetic easy axis with doping,[51] compensation,[29] and strain has been observed in $Ga_{1-x}Mn_xP$, a system with localized, impurity band carriers. Therefore, we conclude that itinerant valence-band holes are not essential for producing anisotropic carrier-mediated exchange interactions. An alternate and useful perspective can perhaps be found in multiband tight-binding calculations[52] which have previously been shown to successfully describe scanning tunnel microscopy experiments between Mn_{Ga} pairs as well as the behavior of *insulating, ferromagnetic* $Ga_{1-x}Mn_xAs$.[17,53] Extension of this model would allow for the calculation of the anisotropy energy due to the relative orientation of the Mn_{Ga} spins and the crystallographic axes.[53]

V. CONCLUSIONS

In summary we have shown a correlation between the perpendicular magnetic anisotropy and epitaxial strain in $Ga_{1-x}Mn_xP$. Growing films in tensile strain by substitution of N for P in the anion sublattice induces the easy axis to lie perpendicular to the film plane. This behavior is reminiscent of that observed in $Ga_{1-x}Mn_xAs$ grown in tensile strain, which suggests a common origin of this effect in the two materials despite differences in band structure and carrier localization. The current viewpoint that magnetic anisotropy in $III_{1-x}Mn_xV$ ferromagnetic semiconductors should be understood in the context of semilocalized valence-band holes may need to be reconsidered to account for the fact that localized, impurity-band holes are capable of mediating

similar anisotropic exchange interactions to those observed in itinerant carrier-mediated ferromagnets. In general, integrating localization effects into models of ferromagnetism is critical to elucidating the fundamental nature of hole-mediated exchange in $III_{1-x}Mn_xV$ materials.

ACKNOWLEDGMENTS

Materials synthesis, x-ray diffraction and SQUID magnetometry experiments at Lawrence Berkeley National Laboratory were supported by the Director, Office of Science, Office of Basic Energy Sciences, Division of Materials Sciences and Engineering, of the U.S. Department of Energy under Contract No. DE-AC02-05CH11231. The FMR work at the Walter Schottky Institut was supported by Deutsche Forschungsgemeinschaft through SFB 631 and the Bavaria California Technology Center. The authors thank R. V. Chopdekar for experimental assistance and C. Bihler, Y. Suzuki, and M. E. Flatté for fruitful discussions. P.R.S. acknowledges support from NSF and NDSEG.

*prstone@berkeley.edu

[1] T. Jungwirth, J. Sinova, J. Masek, J. Kucera, and A. H. MacDonald, Rev. Mod. Phys. **78**, 809 (2006).
[2] S. A. Wolf, D. D. Awschalom, R. A. Buhrman, J. M. Daughton, S. von Molnar, M. L. Roukes, A. Y. Chtchelkanova, and D. M. Treger, Science **294**, 1488 (2001).
[3] X. Liu, W. L. Lim, Z. Ge, S. Shen, M. Dobrowolska, J. K. Furdyna, T. Wojtowicz, K. M. Yu, and W. Walukiewicz, Appl. Phys. Lett. **86**, 112512 (2005).
[4] H. Munekata, A. Zaslavsky, P. Fumagalli, and R. J. Gambino, Appl. Phys. Lett. **63**, 2929 (1993).
[5] X. Liu, Y. Sasaki, and J. K. Furdyna, Phys. Rev. B **67**, 205204 (2003).
[6] A. Shen, H. Ohno, F. Matsukura, Y. Sugawara, N. Akiba, T. Kuroiwa, A. Oiwa, A. Endo, S. Katsumoto, and Y. Iye, J. Cryst. Growth **175-176**, 1069 (1997).
[7] M. Sawicki, F. Matsukura, T. Dietl, G. M. Schott, C. Ruester, G. Schmidt, L. W. Molenkamp, and G. Karczewski, J. Supercond. **16**, 7 (2003).
[8] M. Abolfath, T. Jungwirth, J. Brum, and A. H. MacDonald, Phys. Rev. B **63**, 054418 (2001).
[9] T. Dietl, J. Konig, and A. H. MacDonald, Phys. Rev. B **64**, 241201(R) (2001).
[10] T. Dietl, H. Ohno, and F. Matsukura, Phys. Rev. B **63**, 195205 (2001).
[11] T. Dietl, H. Ohno, F. Matsukura, J. Cibert, and D. Ferrand, Science **287**, 1019 (2000).
[12] M. Glunk, J. Daeubler, L. Dreher, S. Schwaiger, W. Schoch, R. Sauer, W. Limmer, A. Brandlmaier, S. T. B. Goennenwein, C. Bihler, and M. S. Brandt, Phys. Rev. B **79**, 195206 (2009).
[13] M. Sawicki, K.-Y. Wang, K. W. Edmonds, R. P. Campion, C. R. Staddon, N. R. S. Farley, C. T. Foxon, E. Papis, E. Kaminska, A. Piotrowska, T. Dietl, and B. L. Gallagher, Phys. Rev. B **71**, 121302(R) (2005).
[14] K. Alberi, K. M. Yu, P. R. Stone, O. D. Dubon, W. Walukiewicz, T. Wojtowicz, X. Liu, and J. Furdyna, Phys. Rev. B **78**, 075201 (2008).
[15] K. S. Burch, D. B. Shrekenhamer, E. J. Singley, J. Stephens, B. L. Sheu, R. K. Kawakami, P. Schiffer, N. Samarth, D. D. Awschalom, and D. N. Basov, Phys. Rev. Lett. **97**, 087208 (2006).
[16] L. P. Rokhinson, Y. Lyanda-Gellar, Z. Ge, S. Shen, X. Liu, M. Dobrowolska, and J. Furdyna, Phys. Rev. B **76**, 161201(R) (2007).
[17] B. L. Sheu, R. C. Myers, J. M. Tang, N. Samarth, D. D. Awschalom, P. Schiffer, and M. E. Flatte, Phys. Rev. Lett. **99**, 227205 (2007).
[18] P. R. Stone, K. Alberi, S. K. Z. Tardif, J. W. Beeman, K. M. Yu, W. Walukiewicz, and O. D. Dubon, Phys. Rev. Lett. **101**, 087203 (2008).
[19] J.-M. Tang and M. E. Flatte, Phys. Rev. Lett. **101**, 157203 (2008).
[20] R. Farshchi, M. A. Scarpulla, P. R. Stone, K. M. Yu, I. D. Sharp, J. W. Beeman, H. H. Silvestri, L. A. Reichert, E. E. Haller, and O. D. Dubon, Solid State Commun. **140**, 443 (2006).
[21] M. A. Scarpulla, B. L. Cardozo, R. Farshchi, W. M. Hlaing Oo, M. D. McCluskey, K. M. Yu, and O. D. Dubon, Phys. Rev. Lett. **95**, 207204 (2005).
[22] A. Lemaître, A. Miard, L. Travers, O. Mauguin, L. Largeau, C. Gourdon, V. Jeudy, M. Tran, and J.-M. George, Appl. Phys. Lett. **93**, 021123 (2008).
[23] A. W. Rushforth, M. Wang, N. R. S. Farley, R. P. Campion, K. W. Edmonds, C. R. Staddon, C. T. Foxon, and B. L. Gallagher, J. Appl. Phys. **104**, 073908 (2008).
[24] P. R. Stone, J. W. Beeman, K. M. Yu, and O. D. Dubon, Physica B **401-402**, 454 (2007).
[25] O. D. Dubon, M. A. Scarpulla, R. Farshchi, and K. M. Yu, Physica B **376-377**, 630 (2006).
[26] M. A. Scarpulla, O. D. Dubon, O. Montiero, M. R. Pillai, M. J. Aziz, and M. C. Ridgway, Appl. Phys. Lett. **82**, 1251 (2003).
[27] K. W. Edmonds, N. R. S. Farley, R. P. Campion, C. T. Foxon, B. L. Gallagher, T. K. Johal, G. van der Laan, M. MacKenzie, J. N. Chapman, and E. Arenholz, Appl. Phys. Lett. **84**, 4065 (2004).
[28] M. A. Scarpulla, R. Farshchi, P. R. Stone, R. V. Chopdekar, K. M. Yu, Y. Suzuki, and O. D. Dubon, J. Appl. Phys. **103**, 073913 (2008).
[29] P. R. Stone, C. Bihler, M. Kraus, M. A. Scarpulla, J. W. Beeman, K. M. Yu, M. S. Brandt, and O. D. Dubon, Phys. Rev. B **78**, 214421 (2008).
[30] S. Evans, Surf. Interface Anal. **17**, 85 (1991).
[31] Y. K. Yogurtçu, A. J. Miller, and G. A. Saunders, J. Phys. Chem. Solids **42**, 49 (1981).
[32] C. Bihler, M. Kraus, H. Huebl, M. S. Brandt, S. T. B. Goennenwein, M. Opel, M. A. Scarpulla, P. R. Stone, R. Farshchi, and O. D. Dubon, Phys. Rev. B **75**, 214419 (2007).
[33] J. Smit and H. G. Beljiers, Philips Res. Rep. **10**, 113 (1955).
[34] J. Smit and H. P. J. Wijn, Adv. Electron. Electron Phys. **6**, 70 (1954).
[35] C. Bihler, W. Schoch, W. Limmer, S. T. B. Goennenwein, and M. S. Brandt, Phys. Rev. B **79**, 045205 (2009).
[36] J. Kim, D. Y. Shin, S. Lee, X. Liu, and J. K. Furdyna, Phys. Rev.

B **78**, 075309 (2008).
[37] X. Liu, W. L. Lim, L. V. Titova, M. Dobrowolska, J. K. Furdyna, M. Kutrowski, and T. Wojtowicz, J. Appl. Phys. **98**, 063904 (2005).
[38] C. Kittel, *Introduction to Solid State Physics* (Wiley, Singapore, 2005).
[39] S. J. Potashnik, K. C. Ku, R. Mahendiran, S. H. Chun, R. F. Wang, N. Samarth, and P. Schiffer, Phys. Rev. B **66**, 012408 (2002).
[40] C. Gourdon, A. Dourlat, V. Jeudy, K. Khazen, H. J. von Bardeleben, L. Thevenard, and A. Lemaître, Phys. Rev. B **76**, 241301 (2007).
[41] A. Dourlat, V. Jeudy, A. Lemaître, and C. Gourdon, Phys. Rev. B **78**, 161303 (2008).
[42] A. Dourlat, V. Jeudy, C. Testelin, F. Bernardot, K. Khazen, C. Gourdon, L. Thevenard, L. Largeau, O. Mauguin, and A. Lemaître, J. Appl. Phys. **102**, 023913 (2007).
[43] P. T. Chiu, S. J. May, and B. W. Wessels, J. Appl. Phys. **99**, 083907 (2006).
[44] C. Gould, K. Pappert, G. Schmidt, and L. W. Molenkamp, Adv. Mater. **19**, 323 (2007).
[45] V. Novák, K. Olejník, J. Wunderlich, M. Cukr, K. Výborný, A. W. Rushforth, K. W. Edmonds, R. P. Campion, B. L. Gallagher, J. Sinova, and T. Jungwirth, Phys. Rev. Lett. **101**, 077201 (2008).
[46] M. Wang, R. P. Campion, A. W. Rushforth, K. W. Edmonds, C. T. Foxon, and B. L. Gallagher, Appl. Phys. Lett. **93**, 132103 (2008).
[47] D. Hrabovsky, E. Vanelle, A. R. Fert, D. S. Yee, J. P. Redoules, J. Sadowski, J. Kanski, and L. Ilver, Appl. Phys. Lett. **81**, 2806 (2002).
[48] Y. J. Cho, M. A. Scarpulla, Y. Y. Zhou, Z. Ge, X. Liu, M. Dobrowolska, K. M. Yu, O. D. Dubon, and J. K. Furdyna, J. Appl. Phys. **104**, 043902 (2008).
[49] Y. Y. Zhou, X. Liu, J. K. Furdyna, M. A. Scarpulla, and O. D. Dubon, Phys. Rev. B **80**, 224403 (2009).
[50] U. Welp, V. K. Vlasko-Vlasov, A. Menzel, H. D. You, X. Liu, J. K. Furdyna, and T. Wojtowicz, Appl. Phys. Lett. **85**, 260 (2004).
[51] M. Kraus, Diploma thesis, Technische Universität München, 2006.
[52] J.-M. Tang and M. E. Flatté, Phys. Rev. Lett. **92**, 047201 (2004).
[53] D. Kitchen, A. Richardella, J. M. Tang, M. E. Flatte, and A. Yazdani, Nature (London) **442**, 436 (2006).